Experimental Study of Entrainment and Drainage Flows in Microscale Soap Films

Steffen Berg, Eric A. Adelizzi, and Sandra M. Troian*

Microfluidic Research & Engineering Laboratory, School of Engineering and Applied Science, Princeton University, Princeton, New Jersey 08544

Received November 16, 2004

The thickness of freely suspended surfactant films during vertical withdrawal and drainage is investigated using laser reflectivity. The withdrawal process conducted at capillary numbers below 10^{-3} generates initial film thicknesses in the micrometer range; subsequent thinning is predominantly impelled by capillary and not gravitational forces. Under these conditions, our results show that film thinning above and below the critical micelle concentration (cmc) is well approximated by a power law function in time whose exponents, which range from −0.9 to −1.8, are inconsistent with current descriptions of capillary-viscous drainage in inextensible films which predict exponents close to −0.5. Correlations between the experimental fitting parameters illustrate important differences in film behavior across the cmc. In addition, normalization of the drainage data yields a collapse to a single functional form over 3 decades in time for a wide range of initial withdrawal rates. We demonstrate that modification of the interface boundary condition in current models to account for Marangoni stresses through an effective slip parameter yields values of the exponents and other key parameters in excellent agreement with experiment. This modification also successfully describes the withdrawal thickness below the cmc.

I. Introduction

A growing number of theoretical studies have recently focused on entrainment and drainage flows in thin films subject predominantly to capillary and viscous forces (capillary-viscous regime).[1−4] The majority of work in this area stems from the original investigations and modeling efforts of Mysels, Frankel, Lyklema, and others,[5−9] who examined the spectrum of behavior in soap films as a function of surfactant type, concentration, alcohol and salt additives, degradation by-products in water, temperature, and other variables. Despite significant progress in our understanding of thin film behavior since that time,[10−14] there remains a pressing need for more experimental investigations in order to justify the assumptions commonly used in hydrodynamic models. Basic questions involving the actual shape of freely suspended films during steady or transient flows or how the rate of film thinning depends on surface properties have yet to be answered in full.

Several issues complicate direct comparison of experimental results to theoretical predictions. Since very thin films tend to rupture prematurely, it is difficult to collect large data sets from which the extended film shapes and thinning exponents can be extracted in a statistically meaningful way. A second difficulty arises in trying to design experiments which accurately mimic the boundary conditions used in theoretical models such as the interface condition corresponding to a surface of no-slip widely used in analyzing steady film withdrawal.[5] A third complication involves the fact that both entrained and draining films are accompanied by flow instabilities along the film borders (so-called marginal regeneration).[5] To what degree these edge instabilities and not the base states control the film thickness and flow dynamics remains unknown.

The experiments described in this work represent an effort to categorize the entrainment and drainage behavior of freely suspended surfactant films above and below the critical micelle concentration (cmc) through extensive curve fitting and comparison to hydrodynamic models. The first part of this study examines the relation between the entrained film thickness and the capillary number Ca (based on the film withdrawal speed) for $10^{-6} \leq Ca \leq 10^{-3}$. Above the midrange in Ca, the film thickness above and below the cmc is well described by the Frankel relation[5] where $h_0 \sim Ca^{2/3}$. For smaller values of Ca, the film thickness for solutions above the cmc continues to follow the Frankel trend. Below the cmc, the deviations from Frankel's relation can be described by an extended model subject to an effective interfacial slip condition. More importantly, we demonstrate that film thinning for solutions above and below the cmc and throughout the entire range in Ca is well approximated by a single functional form over 3 decades in time. The measured thinning exponents, ranging from −0.9 to −1.8, contrast significantly with recent theoretical predictions (−1/2) of film drainage by capillary-viscous forces in inextensible films.[4,15] Modification of the Frankel analysis to include an interfacial slip condition successfully captures the range in exponents and fitting parameters obtained experimentally. Observed correlations between the experimental

* To whom correspondence may be addressed. E-mail: stroian@princeton.edu. http://www.princeton.edu/~stroian.

(1) Breward, C. J. W.; Howell, P. D. *J. Fluid Mech.* **2002**, *458*, 379.
(2) Schwartz, L. W.; Roy, R. V. *J. Colloid Interface Sci.* **1999**, *218*, 309.
(3) de Gennes, P. G. *Langmuir* **2001**, *17* (8), 2416.
(4) Aradian, A.; Raphael, E.; de Gennes, P.-G. *Europhys. Lett.* **2001**, *55* (6), 834.
(5) Mysels, K. J.; Shinoda, K.; Frankel, S. *Soap Films, Studies of Their Thinning*; Pergamon Press: New York, 1959.
(6) Mysels, K. J.; Cox, M. C.; Skewis, J. D. *J. Phys. Chem.* **1961**, *65*, 1107.
(7) Mysels, K. J.; Cox, M. C. *J. Colloid Sci.* **1962**, *17* (2), 136.
(8) Lyklema, J. *Recl. Trav. Chim. Pays-Bas* **1962**, *81* (9.10), 890.
(9) Lyklema, J.; Scholten, P. C.; Mysels, K. J. *J. Phys. Chem.* **1965**, *69* (1), 116.
(10) Hudales, J. B. M.; Stein, H. N. *J. Colloid Interface Sci.* **1990**, *138*, 354.
(11) Joye, J.-L.; Miller, C. A. *Langmuir* **1992**, *8*, 3083.
(12) Sonin, A. A.; Bonfillon, A.; Langevin, D. *Phys. Rev. Lett.* **1993**, *71* (14), 2342.
(13) Barigou, M.; Davidson, J. F. *Chem. Eng. Sci.* **1994**, *49* (11), 1807.
(14) Langevin, D.; Sonin, A. A. *Adv. Colloid Interface Sci.* **1994**, *51*, 1.
(15) Wong, H.; Fatt, I.; Radke, C. J. *J. Colloid Interface Sci.* **1996**, *184*, 44.

10.1021/la047178+ CCC: $30.25
Published on Web 03/29/2005

Table 1. Solution Properties for Soap Films Used in This Study

solution composition (wt %)	surfactant molarity (mM/L)	surface tension γ (mN/m)	viscosity μ (cP)
2% SDS + 8% glycerol	69.4	35.0 ± 0.5	1 ± 0.1
2% SDS + 4% glycerol	69.4	37.4 ± 0.5	1 ± 0.1
2% SDS	69.4	37.1 ± 0.5	1 ± 0.1
0.4% SDS	13.9	39.1 ± 0.5	1 ± 0.1
0.1% SDS	3.5	45.0 ± 0.5	1 ± 0.1
0.08% SDS	2.8	50.4 ± 0.5	1 ± 0.1

fitting parameters highlight important differences in flow behavior above and below the cmc. We conclude that parametrization of complex Marangoni flows through an effective slip coefficient, as performed here, may prove extremely useful in practical applications where detailed knowledge of surfactant absorption−desorption kinetics or micellar dynamics is unavailable.

II. Experimental Details

A. Materials. All solutions used in this study consisted of sodium dodecyl sulfate (SDS, $C_{12}H_{25}OSO_3Na$, anionic, 99%, Aldrich) and doubly deionized water (18 MΩ cm, Hydro Ultrapure). Some of the solutions above the cmc also contained glycerol (99.5%, Aldrich) in proportions of 4 or 8 wt %. Glycerol typically extends the lifetime of freely suspended films by reducing evaporative effects,[6−8] but recent measurements containing 10% glycerol have also shown a 10-fold increase in the surface viscosity despite a few percentage change in bulk viscosity.[16] The solutions were gently stirred for about 24 h and purified of insoluble particles and contaminants by flowing through a 0.2 μm pore size Nalgene (surfactant-free) disposable filter. The solutions were kept sealed in darkened glass bottles and used within 2 days of preparation. The cmc for SDS in water at room temperature is approximately 0.25 wt %[17] or 8 mM.[18] The corresponding surface tension, γ_{cmc}, is about 37.9 mN/m.[18] In these studies, the surfactant concentration was varied from 0.08 to 2 wt %. Surface tensions were measured by the Wilhelmy plate method;[19] the bulk shear viscosity was measured with a falling ball viscometer. The solution properties are listed in Table 1. In these and previous studies,[20] measurements of the refractive index (Abbe refractometer, ECCI Scientific) of such dilute solutions yielded $n \approx 1.33$. The refractive index of solutions containing 8 wt % glycerol deviated from this value by less than 1%.[21] The value $n = 1.33$ was therefore used throughout the analysis in reconstructing measurements of the film thickness.

B. Fiber Support Assembly. An optically flat square glass cell (5 cm × 5 cm × 8 cm) was first partially filled with 100 mL of soap solution. The cell was then mounted on a vertical stage attached to a single-axis motion controller (US Eurotek, Inc., Laguna Hills, CA). The stage speed could be varied between 0.003 and 20 mm/s over a travel range of 20 mm. The range of accessible capillary numbers was $10^{-6} \le Ca \le 10^{-3}$. A rectangular steel frame connected to a vertical stationary steel column mounted to an independent support for vibration isolation was internally fitted with three 18 μm diameter poly(ethylene terephthalate) (PET) fibers. The three fibers formed an inverted U frame. A sketch of the supporting rectangular frame and internal fiber network is shown in Figure 1a. The lateral spacing between the two vertical fibers could be varied between 4, 10, and 20 mm. All the experiments reported here, with the exception of those in section IIIC, were carried out using a 10 mm fiber separation. The steel frame was then suspended within a glass

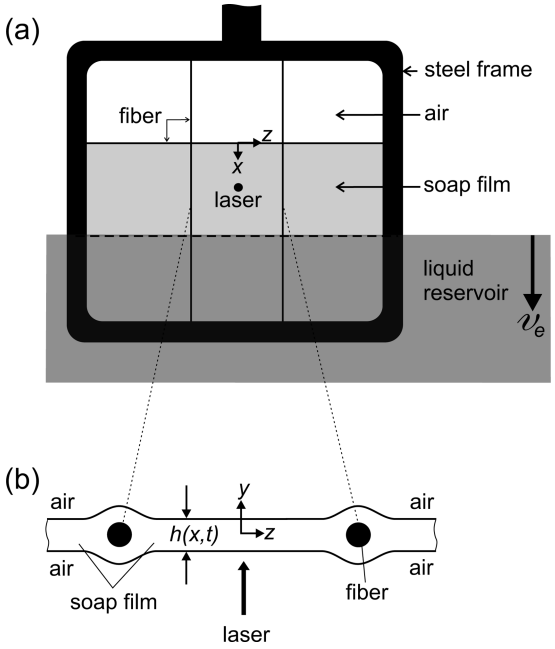

Figure 1. Sketch of freely suspended soap film in (a) front view and (b) in cross section. (a) Soap films were formed on an inverted U frame consisting of three PET fibers (18 μm od). Reflectivity data were obtained at the position of a laser interrogation spot located in the center of the middle film. (b) The symmetric configuration shown and the use of very slender fibers minimized lateral suction into the Plateau borders formed in the vicinity of the two vertical fibers.

cell containing the soap solution. The experiments commenced by positioning the liquid reservoir just above the top horizontal fiber. This geometry normally produced three adjacent soap films in contact with the liquid reservoir. The laser interrogation spot was positioned along the center of the middle film approximately 3 mm below the horizontal fiber, a distance greater than the capillary length. Figure 1b depicts a cross-sectional view of the three adjacent soap films encasing the two vertical fibers. The use of very slender fibers and the symmetric configuration shown helped reduce lateral drainage effects.[8] Visual inspection of the film behavior near these vertical fibers failed to show evidence of sideways flow into the Plateau borders.

Prior to each experiment, all components in contact with the surfactant solutions were first ultrasonically cleaned in a dilute (complelely rinsable) alkaline soap solution (Contrad 70, Decon Laboratories) and dried in a filtered nitrogen stream. The PET fibers were manually strung through small holes drilled into the steel frame. Special care was required to ensure that the horizontal fiber was sufficiently taut to prevent sagging after submersion. The ends of the fibers were taped to the metal frame above the liquid level so as to avoid contact with the soap film or reservoir; the tape was covered by a layer of Parafilm. Numerous tests showed that the PET fibers produced rather consistent and stable films; fibers made of nylon, copper, gold, or nickel−chromium alloy, however, caused premature film rupture. A flexible seal assembled from one finger of a vinyl glove was used to encase and humidify the interior of the glass cell and steel frame. The glass cell and its contents were made to equilibrate within the enclosure for 24 h before being set into motion.

The experimental runs consisted of translating the bulk reservoir downward at a constant speed, v_e, for a total distance of approximately 10 mm. The stage motion was then stopped and the film allowed to drain for several hours. The film thickness was monitored by laser reflectivity from the moment motion commenced until the film ruptured spontaneously after hours of continuous drainage. The stage motion and data acquisition were fully automated allowing for extremely large data sets to be collected remotely. A single experimental run consisted of 3−5 identical experiments programmed for a fixed withdrawal speed,

(16) Martin, B.; Wu, X. L. *Rev. Sci. Instrum.* **1995**, *66* (12), 5603.
(17) Porter, M. R. *Handbook of Surfactants*, 2nd ed.; Blackie Academic and Professional: New York, 1994.
(18) Mysels, K. J. *Langmuir* **1986**, *2* (4), 423.
(19) Adamson, A. W. *Physical Chemistry of Surfaces*; Wiley & Sons: New York, 1976.
(20) Adelizzi, E. A.; Troian, S. M. *Langmuir*, in press.
(21) Lide, D. R. *CRC Handbook of Chemistry and Physics*, 79th ed.; CRC Press: Boca Raton, FL, 1998.

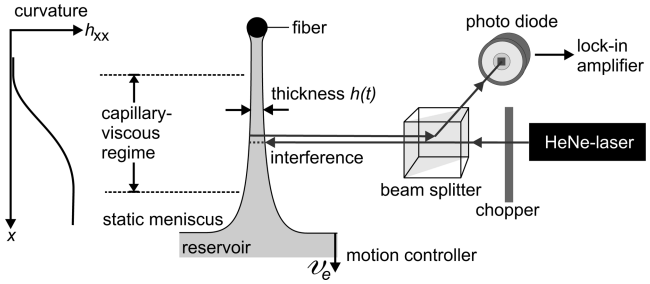

Figure 2. Schematic diagram of experimental setup and film shape corresponding to solution of the Frankel equation. The motion controlled stage supporting a glass cell filled with a soap solution was translated downward at a constant entrainment speed, v_e, for a maximum travel distance of 10 mm. This optical arrangement was used to reconstruct the film thickness during entrainment and drainage. The capillary-viscous regime refers to the portion of the film subject to drainage by gradients in the film curvature, h_{xx}. The static meniscus reflects the region of the film whose (constant) shape is set by the balance of surface tension and gravity. Gravitational forces play no role in the flow dynamics.

v_e, ranging from 0.003 to 10 mm/s. This produced approximately 120−150 measurements of the film thickness with time.

C. Laser Reflectivity Setup. A schematic diagram of the optical assembly is shown in Figure 2. Light from a He−Ne laser (Uniphase, 1 mW, $\lambda = 632.8$ nm) traversed a 50/50 beam splitter striking the soap film at normal incidence. The reflected light was collected by a photodiode (Thorlabs PDA-50), whose output voltage $V(t)$ was used to reconstruct the film thickness with time. A lock-in amplifier (Ithaco 3961B) in combination with a light chopper (1 kHz) improved the signal-to-noise ratio. The analog output of the lock-in amplifier was digitized with an A/D board (PCI-DAS08, Measurement Computing). The entire optical assembly was mounted on a vibration isolation table.

The oscillations in the voltage response of the photodiode represent conditions of maximum constructive and destructive interference in the freely suspended film. A software program was used to identify the peak and trough positions during each run. This identification procedure was further refined by implementing a local parabolic fit to better isolate the corresponding time. Plots of the film thickness in time were then reconstructed from the measured film thickness, $\Delta h = \lambda/4n$, corresponding to adjacent maxima and minima in $V(t)$ starting from the black film limit. Drainage typically proceeded all the way to the Newton black film limit, lasting up to several days before rupture.

The data obtained from a typical run timed at intervals of 10 ms is shown in Figure 3 for a 2 wt % SDS/ 8 wt % glycerol solution entrained at a speed $v_e = 2$ mm/s. The downward displacement of the cell containing the soap solution is shown in Figure 3a. After a total displacement of 10 mm, the film withdrawal process ceased but film drainage continued for several hours. The corresponding output voltage, $V(t)$, is shown in Figure 3b, where the open circles denote the extrema identified by the software program. The corresponding reconstructed film thickness, $h(t)$, is shown in Figure 3c. The inset figure demonstrates the characteristic power law decay observed in these studies. The largest source of error in such measurements was found to arise from the identification of the extrema in $V(t)$. Thicker films, formed at the higher entrainment speeds, produced closely spaced fringes sometimes difficult to isolate neatly. It was found, however, that simultaneous inspection of the voltage curves with the reconstructed profiles helped resolve multiple or missing peaks. To preserve the integrity of the data, all the reconstructed curves for $h(t)$ represent individual runs and not averages obtained at the same entrainment speed.

D. Nonlinear Fitting Procedure for Draining Films. The film thickness was found to be well described by the functional form, $h(t) = h_0^{fit}[1 + \alpha(t - t_0)]^{\beta}$, for solutions above or below the cmc throughout the entire range in Ca examined. Here, t_0, designates the time at which the photodiode first registers a nonzero intensity. The remaining parameters, h_0^{fit}, α, and β, were obtained from a nonlinear fitting routine (applied to a linear

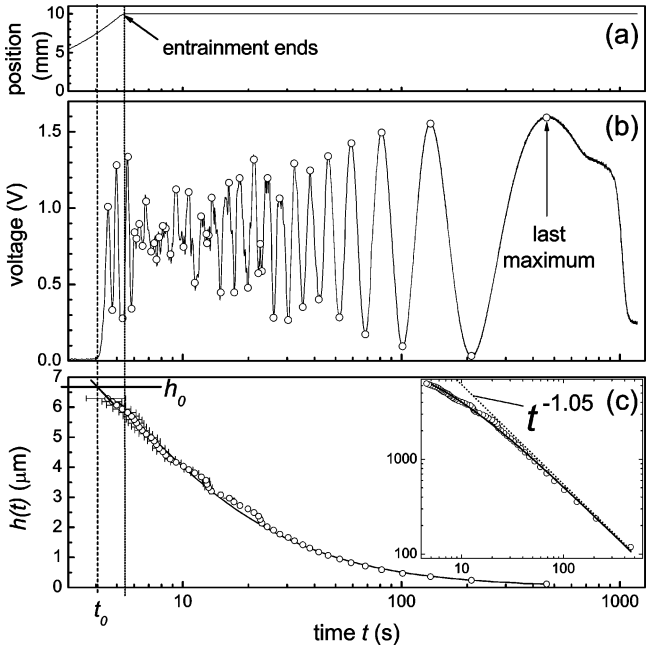

Figure 3. Sample data representing film entrainment and drainage for a solution consisting of 2 wt % SDS and 8 wt % glycerol at an entrainment speed $v_e = 2.0$ mm/s ($Ca = 5.7 \times 10^{-5}$). (a) Position of the liquid reservoir with time. Entrainment ceased at about 5.5 s. (b) Voltage recorded by photodiode detector. The oscillations designate conditions corresponding to maximum constructive and destructive interference. The open circles designate the peak positions determined from the software fitting routine. The last maximum fringe precedes the formation of a black film beyond $t > 1000$ s. (c) Extracted film thickness, $h(t)$, obtained from analysis of the voltage response in (b). The solid line represents the function $h_0^{fit}[1 + \alpha(t - t_0)]^{\beta}$ with $h_0^{fit} = 6.9\ \mu$m, $\alpha = 0.11\ s^{-1}$, $t_0 = 4.1\ s^{-1}$, and $\beta = -1.05$. The experimental value, h_0, corresponds to the film thickness extrapolated to t_0. The inset figure (on a log−log scale) shows the small deviation from power law behavior observed at early times.

time scale) based on a Levenberg−Marquard algorithm.[22] The data points were inversely weighted according to the square of the experimental error determined from the parabolic fit described in the previous section. The initial parameter estimates for h_0^{fit}, α, and β used in initiating the fitting routine were determined as follows. The first two or three data points for $h(t)$ were extrapolated back to t_0 to obtain an initial estimate for h_0^{fit}. The initial value for β was then obtained by fitting the long time data by a single exponent and checking the quality of the fit on a log−log scale. These two estimates then yielded an approximate initial value for α. The final values were extracted from the complete nonlinear fit allowing all three parameters to vary simultaneously. The fitted function was then superimposed on the actual data set and inspected on both linear-linear and log−log scales. The largest deviation from the functional form occurs at earliest times when the film is undergoing entrainment. These deviations were nonetheless always small (see Figure 3c). For all solutions and capillary numbers investigated, the parameter values spanned the following ranges: $0.5 \le h_0^{fit} \le 12\ \mu$m, $0.004 \le \alpha \le 0.3\ s^{-1}$, and $-1.8 \le \beta \le -0.9$. We note that the value h_0, as designated in Figure 3c, corresponds to the entrained film thickness extrapolated back to t_0. The value, h_0^{fit}, instead designates the initial film thickness obtained from the fitting routine as applied to the entire data set.

E. Qualitative Observations. In addition to the interferometric measurements, video recordings of the entire film during drainage revealed some important observations. A digital CCD

(22) Press: W. H.; Teukolsky, S. A.; Vetterling, W. T.; Flannery, B. P. *Numerical Recipes in C*; Cambridge University Press: Cambridge, 1992.

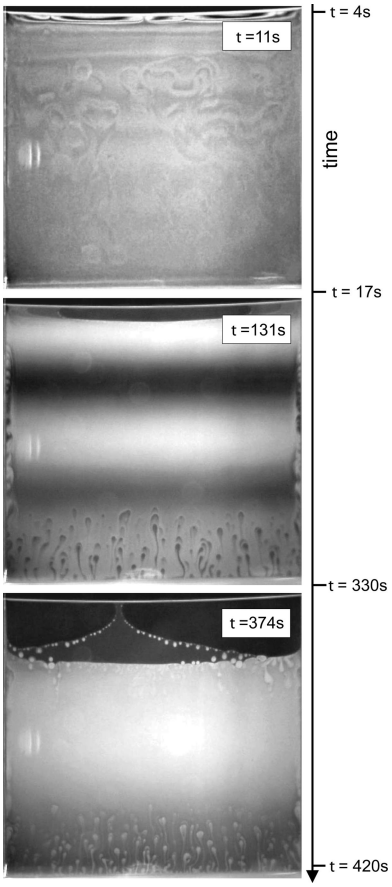

Figure 4. Sequence of images corresponding to a draining film consisting of 2 wt % SDS and 4 wt % glycerol. The film was initially entrained on a frame measuring 2 cm × 2 cm at a speed v_e = 4 mm/s. The time axis to the right designates the interval during which the soap film exhibited the patterns shown. The time stamp within each image designates the actual time at which the image was obtained.

camera (Sony DFW-X700) fitted with a Navitar microscope lens oriented at an angle of 20−40° was positioned behind the film which was diffusely illuminated by a halogen lamp.[23] The video sequences in Figure 4, as well as the interferometry data shown earlier in Figure 3, confirm the evolution of several flow regimes. The time stamps in the upper right corner of each figure designate the time at which the image was obtained. The time markings along the vertical axis designate instead the duration in time over which the phenomena shown were observed.

During the entrainment process, there developed distinct horizontal fringes indicating a thin flat film near the upper fiber and a thicker curved film merging with the bulk solution. Approximately 10−20 s after entrainment had ceased, the horizontal fringes became distorted producing large scale swirling patterns as shown for t = 11 s. These fluctuations rapidly stabilized to produce the orderly fringes shown for t = 131 s. Edge instabilities signifying marginal regeneration, however, developed along the vertical and bottom edge of the film. Inspection of the corresponding data for $V(t)$ revealed that only the points collected at the earliest times were affected by these fluctuations in film thickness. The instability at the bottom edge is believed to arise from a local excess of surfactant created by the drainage process.[24,25] In contrast to earlier studies,[5,10] there did not appear any significant horizontal flow into the Plateau borders at the vertical fibers.

During the later stages of film drainage, there developed a distinct difference in behavior for solutions above and below the cmc. Below the cmc, the soap films continued to drain in regular fashion, simply generating wider interference bands. Solutions above the cmc underwent instead stepwise thinning close to the horizontal fiber leading to Newton black films.[3,14,26−29] This behavior is visible in the upper portion of the image taken at t = 374 s. The thin white horizontal line is the PET fiber. A gray film was observed to coexist with the two black films, whose lower edges appeared decorated with an array of droplets. These three films joined to meet the thicker (white) film while the bottom edge was undergoing marginal regeneration. The interested reader can view elsewhere[30] more detailed color images and an extended video recording of the drainage process.

All the interferometry data were obtained in the stable central portion of the films prior to the black film limit. For solutions above the cmc, however, the region above the interrogation spot normally underwent abrupt thinning transitions. The expelled liquid produced a distinct border joining this portion of the film to the main central region, as seen in Figure 4 for t = 347 s. There was no observable influence on the data collected of this stepwise thinning or border formation except when the black films migrated across the field of view.

III. Experimental Results

The entrainment process establishes the initial conditions for subsequent film drainage. We therefore investigated the dependence of the film thickness during and after withdrawal as a function of the entrainment speed, solution properties and frame size to better assess the mechanisms controlling film thinning in the capillary-viscous regime.

A. Steady-State Film Withdrawal. A.1. Frankel's Law. Mysels, Shinoda, and Frankel[5] were the first to analyze the film thickness and film shapes corresponding to steady withdrawal of freely suspended films at low capillary number. They assumed in their model that the flow dynamics represented a balance between capillary and viscous forces where the liquid viscosity is independent of the shear rate (i.e., Newtonian fluid). They also adopted an interfacial condition for which the film surface translates at the same speed as the frame withdrawal speed v_e. Gravitational drainage was assumed negligible in comparison to capillary drainage, a constraint satisfied provided that the characteristic film thickness, $h_c \ll (\mu v_e/\rho g)^{1/2}$, where μ, ρ, and γ are the solution viscosity, density, and surface tension. Within the lubrication approximation, for which the film thickness is far smaller than its extent, the dimensionless film thickness, H, far from the meniscus where the film is of uniform thickness, was shown to depend on the capillary number, $Ca = \mu v_e/\gamma$, according to

$$H_0 = \frac{h_0}{[\gamma/(\rho g)]^{1/2}} = 1.89Ca^{2/3} \qquad (1)$$

This relation has come to be known as Frankel's law.[7,31] Landau and Levich[32] and Derjaguin[33] had derived earlier a similar relation for vertical film entrainment on a flat and rigid substrate. Bretherton[34] provided the first asymptotic analysis for a film entrained behind a gas

(23) Carlisle, P. http://www.ameritech.net/users/paulcarlisle/soapfilms.html.
(24) Nierstrasz, V. A.; Frens, G. *J. Colloid Interface Sci.* **1998**, *207*, 209.
(25) Nierstrasz, V. A.; Frens, G. *J. Colloid Interface Sci.* **2001**, *234*, 162.
(26) Langevin, D. *Eur. Phys. J. E* **2001**, *5*, 81.
(27) Nikolov, A. D.; Wasan, D. T. *Colloids Surf., A* **1997**, *128*, 243.
(28) Asnacios, A.; Espert, A.; Colin, A.; Langevin, D. *Phys. Rev. Lett.* **1997**, *78* (26), 4974.
(29) v. Klitzing, R.; Espert, A.; Colin, A.; Langevin, D. *Colloids Surf., A* **2001**, *176*, 109.
(30) Berg, S.; Adelizzi, E. A.; Troian, S. M. *Phys. Fluids* **2004**, *16* (9), S6.
(31) Mysels, K. J.; Cox, M. C.; Skewis, J. D. *J. Phys. Chem.* **1961**, *65*, 1107.
(32) Landau, L.; Levich, B. *Acta Physicochim. URSS* **1942**, *17*, 42.
(33) Derjaguin, B. *Acta Physicochim. URSS* **1943** *20*, 349.
(34) Bretherton, F. P. *J. Fluid Mech.* **1961**, *10* (2), 166.

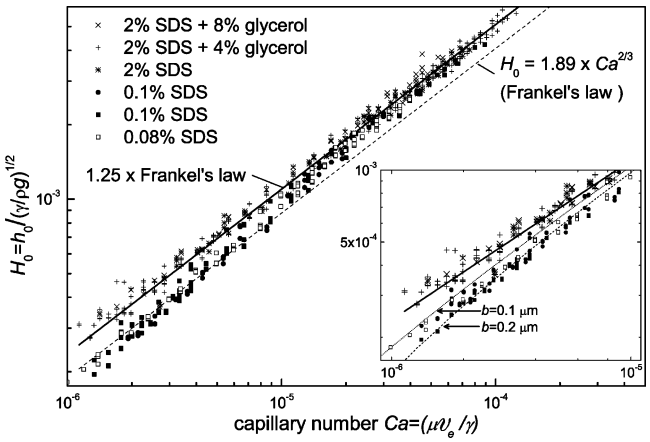

Figure 5. Normalized entrained film thickness, H_0, versus Ca for SDS films (cmc = 0.25 wt %[17]), some of which contain glycerol. The parameter, h_0, denotes the extrapolated film thickness corresponding to t_0, as shown in Figure 3c. For solutions above $Ca \approx 10^{-5}$, the data above and below the cmc lie about 25% above the Frankel relation, $H_0 = 1.89Ca^{2/3}$. Below $Ca \approx 10^{-5}$ and below the cmc (●, ■, □), the data show a monotonic decrease from Frankel's law with decreasing Ca. The inset figure shows a superposition of the data below the cmc with predictions (dashed and dotted lines) of the modified Frankel analysis given by eq 3. The best fits correspond to effective slip lengths in the range $b = 0.1-0.2$ μm.

bubble translating at constant speed in a liquid filled cylindrical tube, where the dominant scaling is also given by eq 1. The film shape corresponding to the Frankel analysis consists of three distinct regions as shown in Figure 1: the static meniscus region characterized by a constant film curvature, $(2\rho g/\gamma)^{1/2}$, a uniform film of thickness h_0 far from the meniscus region, and a transition zone consisting of a film of variable thickness and curvature. The film shape, $h(x)$, in the transition zone reflects a steady flow in which the upward flux caused by the withdrawal process exactly balances the downward flux caused by capillary drainage into the Plateau border of the meniscus region. A matched asymptotic analysis for higher capillary number[35] has shown that eq 1 is valid provided $Ca \lesssim 0.01$.

The appearance of the characteristic length scale $[\gamma/(\rho g)]^{1/2}$ in eq 1 arises only from the matching condition that the film curvature equal the static meniscus curvature at the lower border. The only forces which influence the flow dynamics within the film, however, are viscous and capillary forces not gravity, hence the designation capillary-viscous regime to describe the transition zone. In studies of fiber coating flows, the characteristic length is replaced by the fiber radius. In studies involving small reservoir containers, the characteristic length is set, for example, by the slot opening or other geometric feature size.

All films in this study satisfied the constraint for negligible gravitational drainage. The experimental values, h_0, used to make correspondence with eq 1 were obtained by extrapolation of the entrained film thickness to t_0, as designated in Figure 3c. Figure 5 represents the data for solutions above and below the cmc, including those containing glycerol. Shown in Figure 5 is the extrapolated film thickness, h_0, normalized by the capillary length, $[\gamma/(\rho g)]^{1/2}$, as a function of increasing Ca. The dashed line represents eq 1. For $Ca \gtrsim 10^{-5}$, all solutions, including those containing glycerol, follow the 2/3 Frankel exponent although the film thicknesses are approximately 25% larger than the prediction of eq 1. This enhancement factor may be caused by two effects. The soap film was supported at the top edge by a horizontal fiber whose diameter is several times larger than the entrained film thickness. The corresponding capillary pressure can cause an upward liquid flux leading to slightly thicker films. A second cause of film thickening can arise from an upward directed Marangoni flow,[36-43] which leads to a maximum enhancement of $4^{2/3}$. Fiber coating studies indicate that aqueous SDS solutions above and below the cmc generate thickening factors of 1.0−2.0 for Ca in excess of 10^{-3}.

A.2. Modified Frankel's Law for SDS Films below the cmc. According to Figure 5, the film thicknesses of solutions below the cmc (0.08 and 0.1%) fall progressively below the Frankel scaling with decreasing Ca. This behavior is especially prominent below $Ca \approx 10^{-5}$. The observed deviations, which are beyond the range of experimental error, signal a mechanism causing an additional downward liquid flux and correspondingly thinner films. The presence of surface tension gradients which drain liquid back into the bulk reservoir at sufficiently small entrainment speeds can arise as follows.

The film withdrawal process continually generates fresh interface in the meniscus region connecting the film to the bulk reservoir. Below the cmc, this interface can contain less surfactant than the film regions above it, which due to a longer lifetime maintain a surface concentration in equilibrium with the internal film concentration. The higher surface tension in the meniscus region will then cause fluid to be drained back into the lower reservoir producing thinner films. This net downward flux is expected to increase with decreasing entrainment speed as the Marangoni induced drainage dominates the upward, viscous induced flux.[36-40] A full hydrodynamic analysis describing the flow behavior above and below the cmc and throughout the range of Ca investigated, including micellar kinetics, surfactant adsorption and desorption effects, and Marangoni stresses, is not yet available in the literature.

Recent film studies using associating polymer−surfactant solutions[20,44-46] report the same trend observed in Figure 5 at small values of Ca. Despite the fact that the surfactant concentration in these studies was well above the cmc, complexation effects may retard or inhibit surfactant transport to and from the interface thereby establishing gradients in surface tension. To account for the deviations from Frankel's law, Lionti-Addad et al.,[45] Brunisma et al.,[44] and Adelizzi and Troian[20] have resorted to an effective slip condition to replace the no-slip condition in the usual Frankel analysis. An outline of this analysis is presented below. This slip boundary condition is intended simply as a convenient substitute or "lumped parameter" accounting to first order for the complex interfacial flow engendered by the associating polymer and surfactant micelles. Surprisingly, this simplified treatment successfully describes the deviations from Frankel's law observed at very small values of Ca.

(35) Wilson, S. D. R. *J. Eng. Maths.* **1982**, *16*, 209.
(36) Ratulowski, J.; Chang, H. C. *J. Fluid Mech.* **1990**, *210*, 303.
(37) Park, C.-W. *J. Colloid Interface Sci.* **1991**, *146* (2), 382.
(38) Park, C.-W. *Phys. Fluids A* **1992**, *4* (11), 2335.
(39) Stebe, K. J.; Lin, S.-Y.; Maldarelli, C. *Phys. Fluids A* **1991**, *3* (1), 3.
(40) Stebe, K. J.; Maldarelli, C. *J. Colloid Interface Sci.* **1994**, *163*, 177.
(41) Ramdane, O. O.; Quéré, D. *Langmuir* **1997**, *13*, 2911.
(42) Quéré, D. *Annu. Rev. Fluid Mech.* **1999**, *31*, 347.
(43) Shen, A. Q.; Gleason, B.; McKinley, G. H.; Stone, H. A. *Phys. Fluids* **2002**, *14* (11), 4055.
(44) Bruinsma, R.; di Meglio, J.-M.; Quéré, D.; Cohen-Addad, S. *Langmuir* **1992**, *8*, 3161.
(45) Lionti-Addad, S.; di Meglio, J.-M. *Langmuir* **1992**, *8*, 324.
(46) Cohen-Addad, S.; di Meglio, J.-M. *Langmuir* **1994**, *10*, 773.

Here, we adopt a similar approach to account for the deviations observed in pure surfactant films below the cmc where Marangoni stresses play a key role. As before, the effective slip condition provides a convenient method for parametrizing the counterflow due to Marangoni effects. For the geometry shown in Figure 1a, the Navier-like slip condition[47,48] is given by $v_{slip}(x,y=h) = b(\partial v/\partial y)_{y=h}$, where $(\partial v/\partial y)_{y=h}$ is the fluid shear rate at the free interface and b denotes the slip length (assumed constant at low shear rates[49]). For Marangoni driven flow within the lubrication approximation, the appropriate surface stress condition would be given by $\tau = (d\gamma/dx)_{y=h} = \mu(\partial v/\partial y)_{y=h}$ but solution of the velocity field requires coupling this condition to an equation for the bulk surfactant concentration and the equation of state describing the interface surfactant concentration. The corresponding surface velocity for Marangoni driven flow is then $v_M = h(x)\tau/\mu$, which has been replaced instead by the Navier boundary condition.

The Navier condition is normally applied to liquid−solid interfaces. For the case of freely suspended films, the interfacial velocity is instead given by the difference between the frame withdrawal rate, v_e, and the slip velocity according to

$$v_{x,y=h} = v_e - v_{slip} = v_e - b\left(\frac{\partial v}{\partial y}\right)_{y=h} \quad (2)$$

Following the same analysis which leads to Frankel's law[50] yields a modified equation for the dimensionless entrained film thickness, $H = h(x)/h_0$, namely

$$H_{XXX} = \frac{1 - H}{H^3 + BH^2} \quad (3)$$

where the dimensionless streamwise coordinate retains the Bretherton scaling[34]

$$X = \frac{x}{h_0}(3Ca)^{1/3} \quad (4)$$

Here, the dimensionless slip length is given by $B = 3b/h_0$, which depends implicitly on the entrainment speed through h_0. The conventional surface profile corresponding to the Frankel limit $b \to 0$ is sketched in Figure 2. Equation 3 was solved by a standard Runge−Kutta based shooting technique.[22] The integration proceeded from the linearized solution near $X = 0$ ($H = 1$) to the meniscus region where the curvature approaches a constant value.[5] The parameter B provides the only adjustable parameter in fitting the numerical solutions to the experimental data. The dotted ($b = 0.1\,\mu$m) and dashed ($b = 0.2\,\mu$m) curves shown in the inset of Figure 5 illustrate the best fits bounding the data shown. The numerical solutions describe very well the trend observed with decreasing Ca. Unfortunately, solutions of lower surfactant concentration could not be tested since the films tended to rupture prematurely.

B. Time-Dependent Drainage Flows. As discussed in section II.B, the films continued to drain and thin after film withdrawal ceased. This entrainment process typically lasted from a few seconds to several minutes but film drainage typically proceeded for several hours. As introduced in section IID, the drainage data above and below the cmc could all be fitted by a power law function with the form

$$h(t) = h_0^{fit}[1 + \alpha(t - t_0)]^{\beta} \quad (5)$$

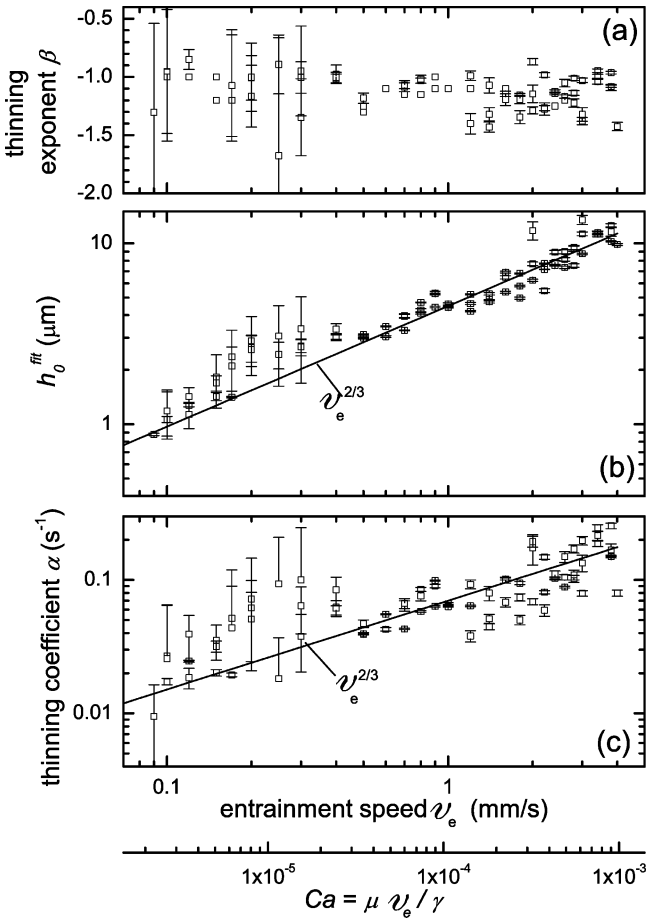

Figure 6. Fitting parameters above the cmc for eq 5 as a function of the initial entrainment speed v_e or equivalently Ca. The films consisted of 2 wt % SDS and 8 wt % glycerol. (Error bars appear larger at small Ca when plotted on a log−log scale.) The solid lines superposed on the data in (b) and (c) represent the scaling relation $v_e^{2/3}$.

The excellent fit was tested on both linear and logarithmic time scales. This functional form approaches exponential behavior at very short times and a simple power law at long times. The parametric studies described below were intended to examine the influence of the initial entrainment speed (or equivalently the initial entrained film thickness) on the fitting parameters, α and β, for solutions above and below the cmc.

B.1. Drainage Parameters above the cmc. The representative data shown in Figure 6 illustrate the dependence of the thinning exponent, β, the initial film thickness, h_0^{fit}, and the thinning coefficient, α, on the entrainment speed, v_e (or equivalently Ca), for solutions containing 2 wt % SDS/8 wt % glycerol. For this example, $-1.4 \lesssim \beta \lesssim -0.9$; within experimental error, this exponent varied little with the entrainment speed. The error bars derive from the nonlinear fitting routine. The initial film thickness, h_0^{fit}, as determined from the nonlinear fit (see section IID), follows the 2/3 exponent predicted by eq 1 for $Ca > 3 \times 10^{-5}$, with small deviations at low Ca. The thinning coefficient, α, shows similar behavior with increasing Ca, including the deviations for $0.09 \lesssim v_e \lesssim 0.4$ mm/s. These deviations, however, are likely the result of

(47) Navier, C. L. M. H. *Mem. Acad. R. Sci. Inst. Fr.* **1823**, *6*, 389.
(48) *Modern Developments in Fluid Mechanics*; Goldstein, S., Ed.; Oxford University Press: New York, 1938.
(49) Thompson, P. A.; Troian, S. M. *Nature* **1997**, *389*, 360.
(50) Probstein, R. F. *Physicochemical Hydrodynamics*, 2nd ed.; Wiley-Interscience: New York, 1994.

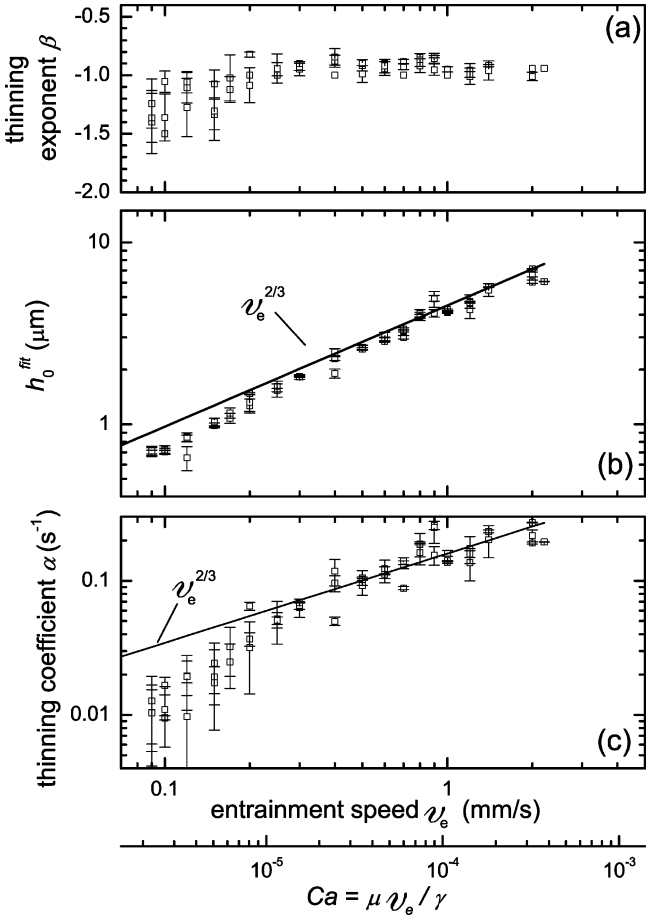

Figure 7. Fitting parameters below the cmc for eq 5 as a function of the initial entrainment speed v_e or equivalently Ca. The films consisted of 0.1 wt % SDS and no glycerol. (Error bars appear larger at small Ca when plotted on a log−log scale.) The solid lines superposed on the data in (b) and (c) represent the scaling relation $v_e^{2/3}$.

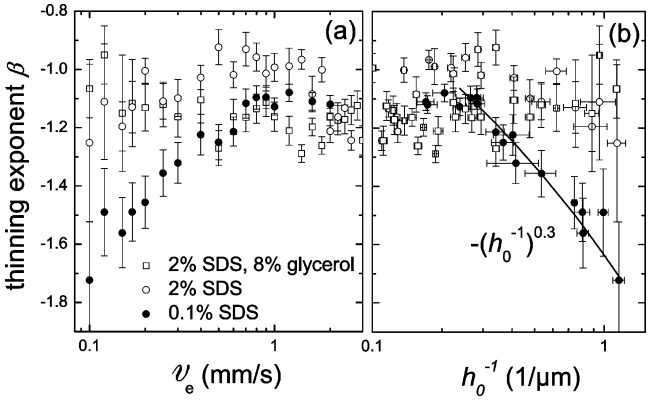

Figure 8. Dependence of the thinning exponent β (see eq 5) on (a) initial entrainment speed v_e and (b) entrained film thickness h_0. Shown are data sets for two solutions above the cmc (□, ○) and one below the cmc (●). (Error bars appear larger at small Ca when plotted on a log−log scale.) The solid curve superposed on the data in (b) represents the scaling relation $\beta \sim -h_0^{-0.3}$.

experimental error since they do not exhibit any reproducible trends. The larger error bars at the smallest entrainment speeds are caused by use of a logarithmic scale as well as use of the entire data set which includes measurements obtained during the entrainment process. These results suggests that for films above the cmc, $\alpha \sim h_0^{fit}$. As discussed further in section III.B.3, the addition of glycerol to solutions above the cmc showed little influence on the dependence of h_0^{fit} and β on Ca but a discernible difference in the behavior of α.

B.2. Drainage Parameters below the cmc. The representative data shown in Figure 7 illustrate the dependence of the thinning exponent, β, the initial film thickness, h_0^{fit}, and the thinning coefficient, α, on the entrainment speed (or equivalently Ca) for solutions containing 0.1% SDS and no glycerol. For entrainment speeds above 0.4 mm/s, the exponent β levels off at a constant value close to unity; h_0^{fit} and α increase in value according to $v_e^{2/3}$. At smaller entrainment speeds, β decreased to a minimum of −1.7. This tendency toward a more negative exponent with decreasing initial entrainment speed indicates more rapid film thinning for smaller Ca. For entrainment speeds $0.09 \lesssim v_e \lesssim 0.4$ mm/s, all three parameters exhibit a systematic downward trend with decreasing Ca. This trend was reproducible and the deviation amplitude larger than experimental error.

B.3. Parameter Trends above and below the cmc. To determine what are the correlations between the fitting parameters, we first examined the behavior of the exponent β as a function of the initial film entrainment speed for solutions above and below the cmc. The value of β was not affected by the vertical position of the laser interrogation spot. Tests in which the laser spot was situated at different positions between the upper horizontal fiber and the bulk liquid reservoir produced variations in β of no more than ±0.1, well within experimental error. Figure 8a illustrates differences in behavior for three types of solutions, namely, two above the cmc (one containing glycerol) and one below the cmc. The data shown for 0.1% SDS represent an average over two solutions prepared at the same concentration. Below an entrainment speed of about 0.5 mm/s, the solutions below the cmc produced more negative values of the thinning exponent β. The lower the entrainment speed, the more negative the value of the drainage exponent. There was no discernible difference in the exponent values for solutions above the cmc with or without glycerol. We replotted the fitted values of the exponent as a function of the initial fitted film thickness, h_0^{fit}, as shown in Figure 8b. There is evidence of a strong correlation below the cmc described by $\beta \sim (h_0^{fit})^{-1/3}$. Above the cmc, the correlation is rather weak and within experimental error.

We tested an additional correlation by examining the dependence of $(\alpha/h_0^{fit})^{asymptotic}$ on the surface tension of the bulk solution. This ratio was obtained in the limit of high entrainment speeds (see inset of Figure 9). The data in Figure 9 show distinctly different behavior above and below the cmc. More importantly, there is also evident a strong influence of the glycerol additive. The parameter α can be regarded as an effective rate constant characterizing the film thinning process. The results shown in Figure 9 suggest that even at the fastest entrainment speeds, films below the cmc drain more rapidly. In addition, glycerol helps slow the drainage but not by increasing the bulk viscosity (see Table 1). This retardation effect may reflect a significant increase in the surface viscosity.[16] This retardation effect is not evident in the behavior of β with increasing entrainment speed, as shown in Figure 8a. Figure 10 provides another confirmation that glycerol affects the surface behavior. When the thinning coefficient is plotted against the initial film thickness, SDS solutions above and below the cmc without glycerol collapse onto the curve $\alpha \propto (h_0^{fit})^{3/2}$. Films above the cmc containing glycerol, however, collapse onto the relation $\alpha \propto h_0^{fit}$.

C. Influence of Frame Size on Drainage Rate. We also examined how the lateral separation of the vertical

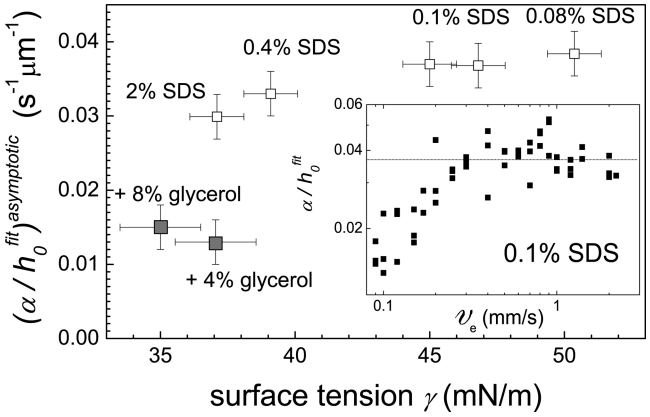

Figure 9. Asymptotic values of the ratio, α/h_0^{fit} (see eq 5), as a function of the surface tension, γ, for all solutions used in this study. The cmc for aqueous SDS solutions is 0.25 wt %;[17] two of the solutions contained glycerol. The sample inset figure shows that a film of 0.1% SDS attains its asymptotic value for α/h_0^{fit} at an entrainment speed $v_e \approx 0.3$ mm/s ($Ca = 6.67 \times 10^{-6}$).

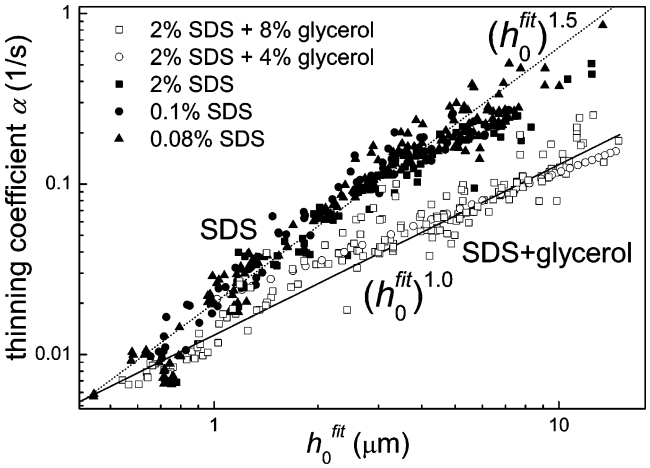

Figure 10. Correlation between the thinning coefficient, α, and the initial film thickness, h_0^{fit}, for three SDS solutions containing no glycerol (solid symbols) and two SDS solutions containing either 4% or 8% glycerol (open symbols). The parameter values α and h_0^{fit} are defined in eq 5. The cmc for aqueous SDS solutions is 0.25 wt %.[17] The pure SDS solutions are fitted by the scaling relation $\alpha \sim (h_0^{fit})^{1.5}$, while the SDS solutions containing glycerol drain more slowly and in accordance with $\alpha \sim (h_0^{fit})^{1.0}$. The data set for the 2 wt % SDS and 8 wt % glycerol film (□) is shown in Figure 6.

fibers on which the soap films form influences the drainage rate. Plotted in Figure 11 are the drainage curves, $h(t)$, for a solution containing 2% SDS/4% glycerol at an entrainment speed of 1.6 mm/s for vertical fiber separations of 4, 10, and 20 mm. The data for 10 and 20 mm spacings are virtually indistinguishable within experimental error indicating negligible finite size effects. The 4 mm spacing generated much thinner films and extrapolation of the entrained film thickness (or likewise the fitted initial thickness) did not obey Frankel's law. In general, frame sizes below 10 mm only affected the value of the initial film thickness, h_0^{fit}, but not the value of the thinning exponent, β, nor the thinning coefficient, α. Since tests of other solutions showed similar results, the majority of experiments were therefore conducted with the 10 mm spacing.

Earlier studies[5,10] have reported that film drainage is either enhanced or even caused by lateral flow into the Plateau borders near the vertical wires, suggesting

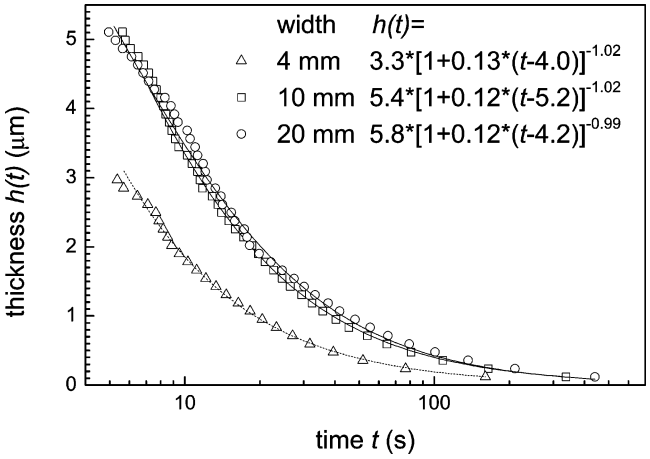

Figure 11. Drainage data, $h(t)$, corresponding to films formed on a frame whose vertical fibers are separated by 4, 10, or 20 mm (see Figure 1). The films consisting of 2 wt % SDS and 4 wt % glycerol were initially entrained at a speed $v_e = 1.6$ mm/s. The data for the two largest separations are virtually indistinguishable within experimental error. The solid curves represent the best fits to eq 5. These fits indicate that decreasing the frame size below 10 mm incluences only the value of h_0^{fit}, but not the values of β or α.

drainage rates inversely proportional to the frame width. This lateral flow is attributed to capillary suction and marginal regeneration. We note two important differences between our work and these earlier studies. Previous experiments investigated the rate of descent of a single interference band as a function of time, where $H_{int}(t)$ denotes the height of the interference band above the bulk reservoir. Such measurements monitor the vertical descent of a fixed thickness film. Our experiments in Figure 11 instead monitor the film thickness, $h(t)$, at a fixed spatial position. Since film thinning is not solely caused by descent of thicker portions of the film, the two measurements do not yield the same dependence on film width. Secondly, as Nierstrasz and Frens[25] have suggested, marginal regeneration along the vertical fibers is likely only a secondary effect of a Marangoni-driven instability within the meniscus region, which may contribute to vertical drainage. Except for very narrow frame widths (e.g., our 4 mm test case), it is therefore expected that measurements of $h(t)$ should not depend significantly on frame width.

D. Self-Similar Behavior above the cmc. As noted in section III.B, films above the cmc for $Ca \geq 3 \times 10^{-5}$ maintain a thinning exponent close to −1.0 independent of the entrainment speed. This should make possible a collapse of the data for this range in Ca. Figure 12 represents the data corresponding to 19 drainage curves for entrainment speeds $0.25 \lesssim v_e \lesssim 3.8$ mm/s for films consisting of 2 wt % SDS/8 wt % glycerol. This collapse is obtained by normalizing the film thickness to the initial value, h_0^{fit}, and by shifting $(t - t_0)$ and rescaling the time axis by α^{-1}. The effective drainage exponent averaged over the entire data set is found to be $\beta = -1.15 \pm 0.1$. A similar collapse occurs for solutions above the cmc not containing glycerol. No such collapse is possible below the cmc where there occurs a systematic increase in $|\beta|$ with decreasing entrainment speed.

This single exponent above the cmc indicates that the mechanism responsible for film thinning is independent of the entrainment film thickness. This observation suggests the possibility of a simplified equation to explain the self-similar behavior. As discussed in section IV.A, however, the experimental values of the thinning expo-

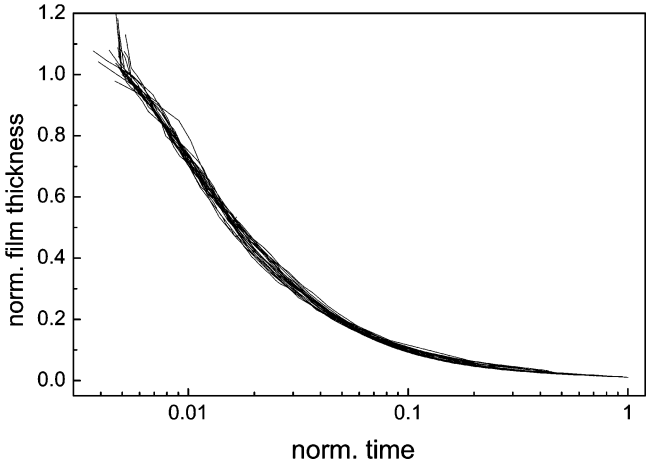

Figure 12. Superposition of normalized drainage curves for solutions initially entrained at speeds $0.25 \lesssim v_e \lesssim 3.8$ mm/s for films consisting of 2 wt % SDS and 8 wt % glycerol. (This same data set is shown in Figure 6.) The film thickness and drainage times have been rescaled based on the form of eq 5. The average thinning coefficient is $\beta = -1.15 \pm 0.1$.

nent, which range from -0.9 to -1.8, are inconsistent with current descriptions of capillary-viscous drainage in inextensible films which predict exponents close to -0.5.[4,15] Our findings suggest that Marangoni effects, which occur spontaneously during drainage flow, contribute significantly to the thinning rate both above and below the cmc. We review next the predictions of current models and suggest how incorporation of an effective slip condition into the hydrodynamic analysis for film thinning by capillary and viscous forces captures the experimental trends described.

IV. Discussion

The demonstrated agreement of the entrained film thickness for films above the cmc with Frankel's relation for steady flows in the range $10^{-6} \lesssim Ca \lesssim 10^{-3}$ supports the approximations used in obtaining eq 1. Below the cmc, we showed in section III.A.2 that substitution of an effective Navier slip condition for the usual no-slip boundary condition captures the correct behavior of the entrained film thickness with decreasing Ca. After reviewing the range of exponents predicted by current models, we show that a similar approach can be used to describe the time-dependent drainage flow of a freely suspended film. Replacement of the conventional no-slip by an effective slip boundary condition yields thinning exponents in agreement with the experimental results. The effective slip lengths corresponding to film drainage are approximately an order of magnitude smaller than the characteristic film thickness.

Prior studies of drainage by capillary and viscous forces have mostly focused on thin horizontal films where capillary suction near the Plateus border causes a characteristic dimple near the film edge.[3,11] Frankel and Mysels[51] investigated the thinning of an interstitial film trapped between two coalescing droplets. They compared their results to the Reynolds lubrication model for the squeeze flow[52,53] imparted by two rigid parallel disks approaching at constant force. The Reynolds equation predicts that $-\mathrm{d}h/\mathrm{d}t \propto t^{-3/2}$, or equivalently, $h(t) \propto t^{-1/2}$, for a flat liquid film made to thin by a constant normal force. Findings of a similar -0.5 exponent in later experiments on freely draining films were also incorrectly attributed to the Reynolds analogy. Barigou and Davidson[13] finally and correctly explained, however, that the Reynolds formula significantly underestimates drainage rates by several orders of magnitude because the mechanism for film thinning in deformable or free interface films is unrelated to squeeze flow. Essentially, the Reynolds analysis assumes the absence of tangential stresses, which Barigou and Davidson argued contribute substantially to drainage in soap films.

Cohen-Addad and di Meglio's[46] studies on vertically draining films of 2% aqueous SDS showed that $-\mathrm{d}h/\mathrm{d}t \sim t^{-2}$ or equivalently $h(t) \propto t^{-1}$. Barigou and Davidson[13] conducted a number of drainage experiments in horizontal geometry with different surfactant solutions. A fit of their data as reported in Figure 6 of ref 8 (commercial detergent 5 vol %, distilled water 95%, 0.02 M KCl) to eq 5 yields an exponent $\beta \approx -0.7$. Hudales and Stein[10] conducted studies of vertically draining films of CTAB (cetyltrimethylammonium bromide, cationic) above the cmc which were supported on a glass frame much thicker than the dimensions of the fibers used in the present study. From the data reported in ref 10, $-1.2 \le \beta \le -1.0$. The range of exponents obtained in these earlier studies is therefore consistent with those reported in this work.

There exist only a few theoretical studies describing film thinning in the capillary-viscous regime, all of which neglect Marangoni effects. Wong, Fatt, and Radke[15] proposed a model for the thinning of a tear film caused by the retraction of the eye lid after blinking. The boundary and initial conditions were different than those normally used in the Frankel analysis. Nonetheless, their results showed rapid thinning in the region described by significant film curvature, $h_{xxx,t}$. The diminishing film thickness at this "pinch point" was found to scale at late times as $t^{-0.46}$. Using different boundary and initial conditions, Aradian and de Gennes[4] derived from a self-similar analysis that the diminishing film thickness should generally scale as $t^{-1/2}$.

As shown next, film drainage in the capillary-viscous regime which proceeds from an initial (Frankel) shape governed by eq 3 (with $B = 0$) generates the scaling relation $h(t) \sim t^{-1/2}$ within the transition zone. Drainage from initial profiles where $B \neq 0$ generate thinning exponents in excellent agreement with experiment.

A. Capillary-Viscous Drainage Subject to an Effective Slip Condition. Consider first the dimensionless evolution equation describing the time-dependent thinning of a freely suspended film subject to capillary and viscous forces where there is no interfacial velocity and no shear stress along the film center

$$H_\tau + (H_{XXX}H^3)_X = 0 \tag{6}$$

The dimensionless time is defined by $\tau = t/t_c$ where $t_c = 3\gamma\mu/(\rho^2 g^2 h_0^3)$; the dimensionless streamwise coordinate is defined by $X = x/l_c$ where $l_c = [\gamma/(\rho g)]^{1/2}$ is the capillary length characterizing the static meniscus region. The subscripts in eq 6 represent partial derivatives with respect to τ and X, respectively. For films formed by prior entrainment at constant speed, where the Frankel scaling is observed to hold, one can realistically assume an initial condition corresponding to a Frankel profile.[5] The coordinate corresponding to the flat film limit far from the meniscus is designated by $X = 0$. To better approximate the geometry of the experimental films which exhibit film curvature near the upper horizontal fiber and near the bottom liquid reservoir, the numerical solutions were initiated from a "twinned" Frankel profile, which ensured

(51) Frankel, S. P.; Mysels, K. J. *J. Phys. Chem.* **1962**, *66* (1), 190.
(52) Reynolds, O. *Philos. Trans. R. Soc. London* **1886**, *177*, 157.
(53) Sheludko, A. *Adv. Colloid Interface Sci.* **1967**, *1*, 391.

symmetry about $X = 0$ and no curvature in the flat film regime. The boundary conditions applied at the upper and lower domain boundaries were $H_{XX} = 0.64$ and $H_{XXX} = 0$.[5,50]

The numerical solutions were computed by the method of lines.[54] As expected from eq 6, film thinning initiates near points where $H_{XXX,\tau}$ is largest. Numerical solutions of the thinning profile near the flat film region, $H(\tau)$, were successfully fitted by eq 5 with $\beta = -0.472 \pm 0.001$. This exponent, which did not vary significantly with position X, agrees with previously reported values despite the use of different initial and boundary conditions.[4,15] This suggests that the exponent represents the balance of capillary and viscous forces and that its value is not so sensitive to the initial conditions assumed. The numerical solutions corresponding to the film thickness in the flat film regime, where the changes in curvature are vanishingly small, could not be fit by eq 5; the asymptotic behavior in this regime, however, scaled as $H \sim \tau^{-0.2}$. Comparison of the drainage times in the flat film region obtained numerically with the experimental time scales accessible to our apparatus confirmed that the reflectivity data represent film drainage in the transition zone. This first numerical exercise therefore establishes that capillary-viscous drainage in inextensible films typically produces drainage exponents close to a value $-1/2$.

This procedure was then repeated using an evolution equation corresponding to the Navier slip boundary condition

$$H_\tau + [H_{XXX}(H^3 + BH^2)]_X = 0 \qquad (7)$$

using similar boundary and initial conditions for the film shape as described above. A dimensionless slip length $B = 10$ yielded a thinning exponent $\beta \approx -1.1$, in agreement with the measured values for films above the cmc. For $B = 10$, the value of the slip length, b, is more than triple the initial film thickness. This establishes the presence of a significant downward liquid flux likely due to surface tension gradients generated spontaneously during the drainage process. The slip lengths, b, corresponding to the entrainment data for films below the cmc (where $B = 0.03-2.3$), were found to be much smaller than the slip lengths corresponding to pure drainage flow above and below the cmc. This observation strongly suggests that Marangoni effects contribute more significantly to pure drainage flow in freely suspended films. The values for β obtained from the numerical simulations also produced correspondingly accurate values for the thinning coefficient α. As an additional test, sample profiles different from the Frankel shape were input as initial conditions to eq 7 with the result that the thinning exponent β was always still of order 1. No matter what film shape was input as an initial condition, however, it was not possible to recover accurate values for β if the effective slip condition was set to zero. This last finding confirms that spontaneous Marangoni flows established during the drainage process cannot be ignored.

V. Conclusions

The influence of gradients in surface tension on steady film entrainment and unsteady drainage in the capillary-viscous regime are difficult to assess a priori. Marangoni stresses can arise below the cmc thereby contributing significantly to film thinning or thickening. Variables affecting the degree of surface stress include the speed of entrainment or drainage, the frame type, size or geometry used to support the freely suspended film, the type of surfactant used and its concentration, and surfactant degradation products such as alcohols which can act as cosurfactants. Prior studies of film entrainment have demonstrated a rich and complex assortment of behavior depending on the kinetics of surfactant adsorption and desorption, the dynamics of micellar formation and dissolution, and the convective time scale set by the entrainment speed.[36]

The experiments reported here describing steady entrained flow for $10^{-6} \leq Ca \leq 10^{-3}$ indicate that an extended version of Frankel's analysis incorporating an effective slip condition is successful in describing the deviations in film thickness below the cmc. The extracted slip length is approximately an order of magnitude smaller than the entrained film thickness. A similar change in boundary condition successfully describes the thinning exponents measured in unsteady drainage flow. Solutions above and below the cmc parametrized in this way yield effective slip lengths approximately triple the initial film thickness. These results signify a substantial drainage flux induced by Marangoni effects above and below the cmc. These results are somewhat expected since the externally applied entrainment speed far exceeds the spontaneous drainage flow achieved after entrainment ceases. The slower the characteristic flow speed, the larger the potential contribution from Marangoni effects. More detailed analysis of the interferometric data reveal that a function of the form $h_0^{\text{fit}}[1 + \alpha(t - t_0)]^\beta$ successfully describes the drainage behavior above and below the cmc. This form represents a smooth transition from exponential behavior at early times to a power law behavior at long times. Correlations among the fitting parameters, h_0^{fit}, α, and β, provides further insight into the drainage dynamics, including the influence of glycerol, which at low concentrations significantly slows drainage through an increase in the surface viscosity with little change in bulk viscosity.

Conventional hydrodynamic studies of soap films require a complete description of surfactant adsorption/desorption effects as well as an accurate equation of state relating the surface tension to the local bulk concentration. In the absence of such detailed information, these experiments indicate that is it nonetheless possible to extract important information about film entrainment thickness and drainage rates by way of an effective slip parameter. Further tests involving different types of surfactant or associating polymer−surfactant solutions will hopefully support this simplified view.

Acknowledgment. The authors gratefully knowledge financial support from Unilever Research US, the National Science Foundation (CTS and DMR programs), and the NASA Microgravity Fluid Physics Program. S.B. wishes to thank A. A. Darhuber, T. D. Dimitrova, and B. Schäfer for helpful discussions and Professor Bud Homsy for suggesting recent literature on thickening factors. S.M.T. kindly acknowledges the warm hospitality and generous support of the Moore Distinguished Scholar Program at Caltech where this work was completed. The authors also wish to thank one of the reviewers for an especially thorough reading of this manuscript.

(54) MATLAB 6.5 (R13), The MathWorks Inc.

LA047178+